LAWRENCE
LIVERMORE
NATIONAL
LABORATORY

LLNL-CONF-562376

Integrating Work in Seismic Attenuation, Coda Decay, and Source Models for Event Identification and Characterization

M. E. Pasyanos, W. R. Walter, E. M. Matzel, R. Gok, S. R. Ford, H. Xu, K. M. Mayeda

June 25, 2012

Monitoring Research Review
Albuquerque, NM, United States
September 18, 2012 through September 20, 2012

Disclaimer

INTEGRATING WORK IN SEISMIC ATTENUATION, CODA DECAY, AND SOURCE MODELS FOR EVENT IDENTIFICATION AND CHARACTERIZATION

Michael E. Pasyanos[1], William R. Walter[1], Eric M. Matzel[1],
Rengin Gök[1], Sean R. Ford[1], Heming Xu[1], and Kevin Mayeda[2]

[1]Lawrence Livermore National Laboratory
Sponsored by National Nuclear Security Administration
Contract No. DE-AC52-07NA27344/LL12-Source_Physics-NDD02

[2]University of California, Berkeley
Sponsored by National Nuclear Security Administration
Contract No. DE-AC52-07NA27344/LL12-Source_Physics-NDD02

ABSTRACT

For the past number of years, Lawrence Livermore National Laboratory has been developing a wide variety of research products for use in nuclear explosion monitoring. These include coda calibration for magnitude determination, attenuation models for amplitude prediction, velocity models like RSTT and LLNL-G3D for predicting travel times, as well as earthquake and explosion source models. Here, we present on work we have done integrating all of these products in the creation and modeling of regional waveform envelopes across a broad frequency band. By specifying the noise levels, along with arrival times, source amplitudes, propagation (geometrical spreading and attenuation) effects and coda decay parameters for the regional phases (Pn, Pg, Sn, Lg), we can construct envelope templates, which can be compared to the observed envelopes. This represents an effort to use more of the waveform than parametric information, such as travel times or magnitudes, but not attempting the difficult task of trying to fit the whole waveform, swing-for-swing, at high frequencies. This method has applications for event identification, depth determination, magnitude estimation, and more sophisticated analysis, such as estimating the yield and depth-of-burial of explosions. We will first report on the progress we are making on many of the individual constitutive products, such as the high-resolution attenuation tomography of the crust and upper mantle that we are developing for Eurasia. For earthquakes, we use the MDAC source model while, for explosions, we explore the Mueller-Murphy model and proposed extensions of the model for S-waves, and explosion source spectral models based on modifications to the Denny-Johnson model. We will then illustrate how we are utilizing the methodology to characterize events in the Korean Peninsula and at the Nevada National Security Site (NNSS, formerly known as the Nevada Test Site).

OBJECTIVES

Our objective is to integrate work in seismic attenuation, coda decay, and source models in order to improve out ability to identify events as either earthquakes or explosions, and then further characterize their source attributes, such as depth and seismic yield. Improvements to many of these individual elements has allowed us to develop a new method of fitting significantly more of the waveform with envelopes over a broad frequency band, with potential payoff in event identification and characterization.

RESEARCH ACCOMPLISHED

In the past year, we have accomplished a number of research goals: improved regional attenuation maps in Eurasia, demonstration of event discrimination (calibrated high-frequency P/S discriminants) over broad regions, and the development of a new method of using regional waveform envelopes for event identification and source characterization, shown here for events in the Korean Peninsula and at the Nevada National Security Site (NNSS, formerly known as the Nevada Test Site). We will also discuss how the attenuation models are used in capability analysis, including extensions of the method to coda phases.

Seismic Attenuation

LLNL has developed a four-phase amplitude tomography which allows us to determine a set of attenuation, site, and source corrections for the primary regional phases of Pn, Pg, Sn, and Lg. Our basic methodology, employed in Pasyanos et al. (2009a) for Lg, uses an MDAC source model (Walter and Taylor, 2001), which more explicitly defines the source expression in terms of an earthquake source model formulated in terms of the seismic moment. We applied the technique to simultaneously invert amplitudes of Pn, Pg, Sn and Lg in the Middle East to produce P-wave and S-wave attenuation models of the crust and upper mantle for the region (Pasyanos et al., 2009b).

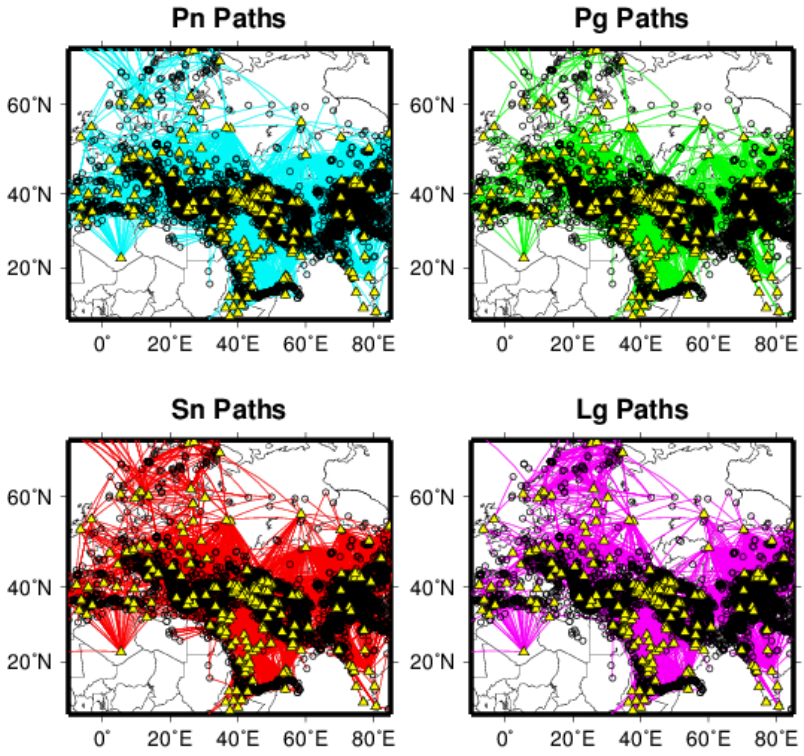

Figure 1. Path map of Pn, Pg, Sn, and Lg attenuation measurements for western and central Eurasia in the 1-2 Hz passband.

We have extended the region into Europe to cover all of western Eurasia and portions of north Africa, as shown by the path maps in Figure 1. The attenuation is modeled as P-wave and S-wave attenuation layers for the crust, and a similar set for the upper mantle. Inverting all of the phases simultaneously allows us to determine consistent attenuation, site, and source terms for all phases, and eliminates non-physical inconsistencies among them. Attenuation results are shown in Figure 2.

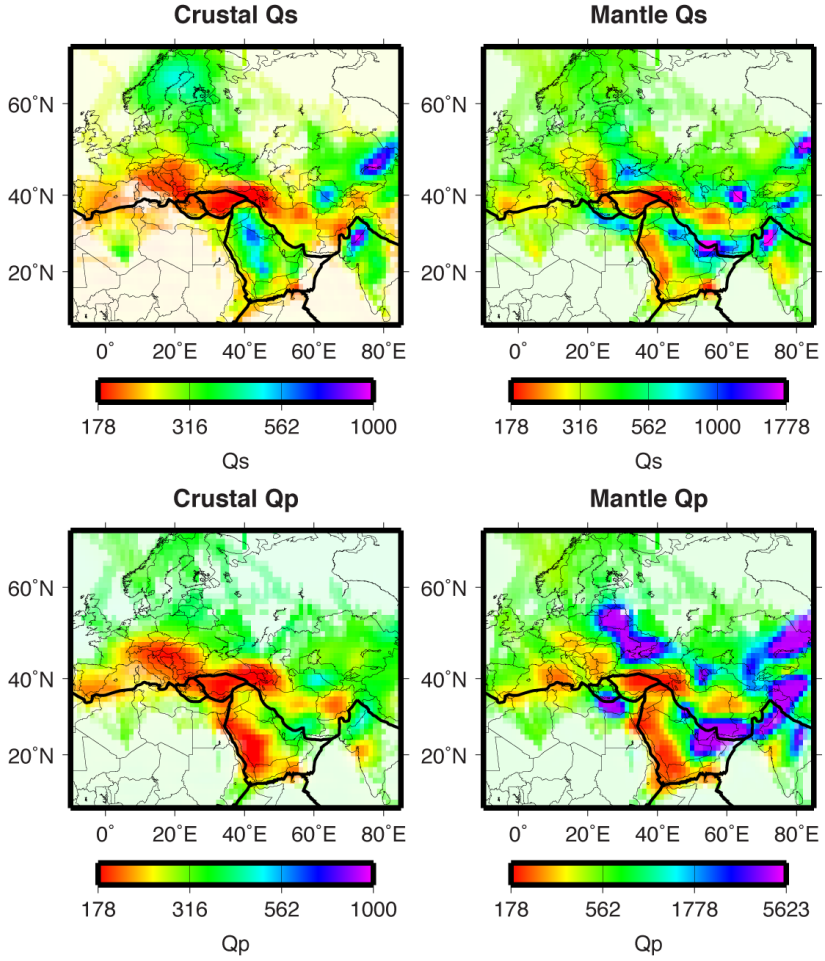

Figure 2. Attenuation of crustal Qs, mantle Qs, crustal Qp, and mantle Qp of western and central Eurasia in the 1-2 Hz passband.

It has been demonstrated that applying corrections with the attenuation models can significantly improve earthquake-explosion discrimination using high-frequency regional P/S amplitude ratios (Pasyanos and Walter, 2009). P/S discriminants are expressed as the ratio between the P-wave amplitude (A^P) and the S-wave amplitude (A^S) and, because of the large variations, are usually plotted on a log scale. To correct the phase ratio for path and source effects, we adjust the individual amplitudes assuming an earthquake source. We then form our discriminant using the ratio of the corrected amplitudes:

$$\text{discriminant} = \log\left[\frac{(A^P / A_0^P)}{(A^S / A_0^S)}\right] = \log\left[\frac{A^P}{A^S}\right] - \log\left[\frac{A_0^P}{A_0^S}\right] \qquad (1)$$

where A_0 are the amplitude predictions for an earthquake of that phase and size. As a result, the corrected discriminant should now have a value around 0 (P/S ratio of 1) for earthquakes. We input a best estimate of the earthquake size by using a moment magnitude, if available, or otherwise estimating Mw using other magnitude estimates.

We have tested the use of the 2-D attenuation model for discrimination over broad regions by using data from the historical Borovoye dataset (Kim and Ekstrom, 1996; Baker et al., 2009) which has recorded dozens of events from the Semipalatinsk Test Site, as well as Peaceful Nuclear Explosions (PNEs) from the broader region. Figure 3 shows an example of the good separation that is achieved between earthquakes and explosions with Pn/Sn in the 4-6 Hz passband using corrections from the attenuation model. Only a known overburied PNE does not separate well from the earthquakes at this frequency (Pasyanos et al., 2012a) and the explosion-like presumed earthquakes are coming from a known mine region (Hans Hartse, personal communication). The improvements using 1-D and 2-D corrections are quantified in the right panel, which shows increasing Mahalanobis distance and reduced equiprobable points at all frequency bands using the 2-D model. The overall discrimination performance and improvements using the 2-D model are most significant at 2-4 Hz.

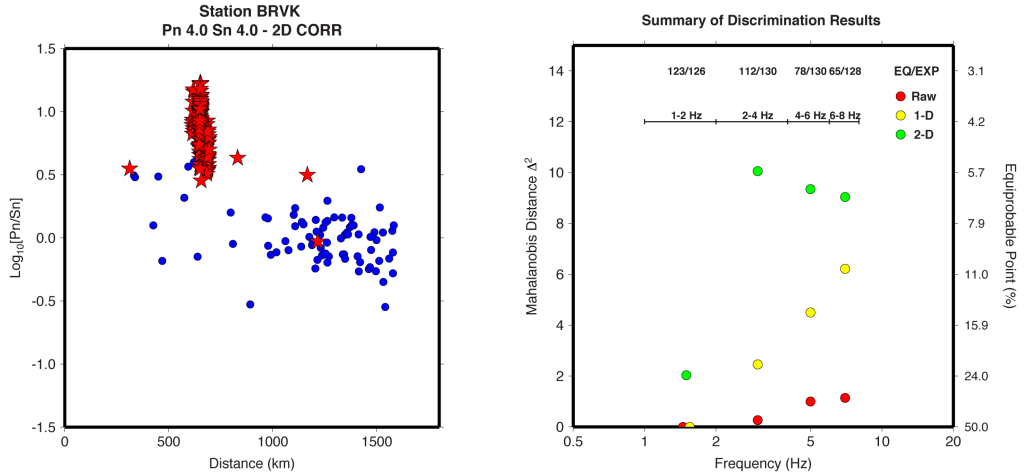

Figure 3. The left figure shows corrected Pn/Sn ratios of earthquakes (blue circles) and explosions (red stars) recorded at station Borovoye. Explosions included nuclear tests from the Semipalatinsk Test Site as well as PNEs from the broader region. The right figure shows a comparison of discrimination performance (in both Mahalanobis Distance and equiprobable point) at various frequencies using raw ratios, 1-D corrected ratios, and 2-D corrected ratios. Figure from Pasyanos et al. (2012a).

Coda shape

To create model amplitude envelopes, we will be employing the Coda Wave Method (Mayeda and Walter, 1996; Mayeda et al., 2003). With this technique, the analytic expression that we used to fit the observed narrowband envelopes at the center frequency f as a function of distance r (in kilometers) for times greater than the direct *S*-wave arrival is

$$A_c(f, t, r) = S(f) \bullet U(r,f) \bullet P(f) \bullet T(r, f) \bullet H(t - r/v(r)) \bullet (t\text{-}r/v(r))^{-\gamma(r)} \bullet \exp[b(r) \bullet (t\text{-}r/v(r))] \quad (2)$$

where S(f) is the source amplitude, U(r,f) is the propagation (geometrical spreading and attenuation), P(f) is the site response, T(f) is the direct phase-to-coda transfer function. H is the Heaviside step function, t is the time in seconds from the origin, r is the epicentral distance in km, v(r) is the velocity of the peak arrival in km/sec, and $\gamma(r)$ and b(r) are coda shape parameters, which can be complicated functions of frequency and distance.

Calibration of coda in the Middle East and other areas is complicated by the fact that the dominant S-wave phase varies depending on tectonic region, distance, and frequency. This past year, we have been improving coda calibrations in the Middle East, including lateral variability in the attenuation and coda decay parameters across the region.

Source Models

For earthquake source spectra, we make use of the MDAC source model (Walter and Taylor, 2001), that is a more generalized form (encompassing P, S-waves and variable apparent stress) of the well-known and widely used Brune (1970) model. The minimum input parameter would be a seismic moment Mo although, if available, additional source parameters such as apparent stress could be input to provide a more accurate source term. For explosions, we explore the use of several models. First, we will make use of the Mueller-Murphy model (Mueller and Murphy, 1971) for P-waves, which produce a source model for a specified depth, yield, and choice of emplacement media (e.g., granite, salt, tuff, or shale). For explosion S-waves, we make use of the Fisk conjecture which posits that "S-wave corner frequency is reduced by the ratio of near-source shear and compressional velocities" (Fisk, 2006). The S-wave corner frequency, low frequency level and high frequency falloff remain areas of active research.

Ford et al. (2012) developed a parametric model of the nuclear explosion seismic source spectrum derived from regional phases, using data from the Nevada and Semipalatinsk Test Sites. Source spectra are fit with a generalized version of the Brune spectrum, which uses a three-parameter model (long-period level, corner-frequency, and spectral slope at high-frequencies). The parameters are then correlated with near-source geology and containment conditions. We will be testing the model of Ford et al. (2012) and other explosion source spectral models based on modifications to the Denny-Johnson model (Denny and Johnson, 1991).

Regional Amplitude Envelopes

We consider a less empirical, more physics-based method of fitting the complete regional amplitude envelope. The full regional waveform envelope in a given frequency band can be described as the sum of the noise and all of the regional phase envelope amplitudes or:

$$A_{total} = A_{noise} + A_{Pn} + A_{Pg} + A_{Sn} + A_{Lg} \qquad (3)$$

where A_{noise} is the noise level in that frequency band, and A_{Pn} and A_{Sn} are zero at local distances where these phases are non-geometric. The regional phase terms (A_{Pn}, A_{Pg}, A_{Sn}, A_{Lg}) include the direct phase and coda can be described as:

$$A = A_{direct} \bullet H(t-t_a) \bullet (t-t_a)^{-\gamma(r)} \bullet \exp(b \bullet (t-t_a)) \qquad (4)$$

where A_{direct} is the direct phase amplitude. This is the same form as equation (2) above, but with direct amplitudes (which include source, propagation, and site terms) replacing the first four terms used earlier. The only term not directly incorporated in the direct phase amplitudes is the transfer term T(f), which we will be considering more later. We have also replaced r/v(r) with the arrival time t_a.

Conceptually, this is shown in Figure 4, where the envelopes will have a sawtooth pattern from the arrival and decay of local and regional phases. The amplitude of the direct phase may be sensitive to factors such as radiation pattern, directivity, path propagation, and multipathing. The direct phase however only represents a relatively short segment of the overall envelopes, and are only important for setting the overall coda levels, which are not sensitive to these same factors.

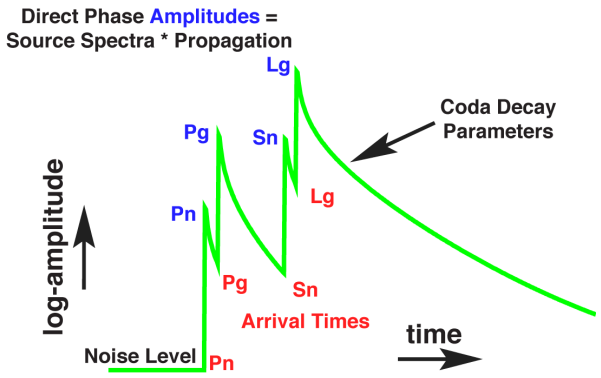

Figure 4. Illustration of expected envelope shapes for regional events. The plot shows logarithmic velocity variation as a function of time and the sawtooth pattern comes from the arrival and decay of prominent regional phases. Figure from Pasyanos et al. (2012a).

Changes in moment and corner frequency (for earthquakes) and changes in the yield, depth, or material properties (for explosions) will change the source spectra, which will result in differences to the synthetic coda envelopes, as illustrated in Figure 5. The top panels show the affect of changes to seismic yield on the moment spectra and the 2-3 Hz envelopes. The bottom panels show the effect of changes to depth of burial. Notice the increase in amplitudes for the intermediate depth (500 m) in this particular frequency band; this would not happen at higher and lower passbands.

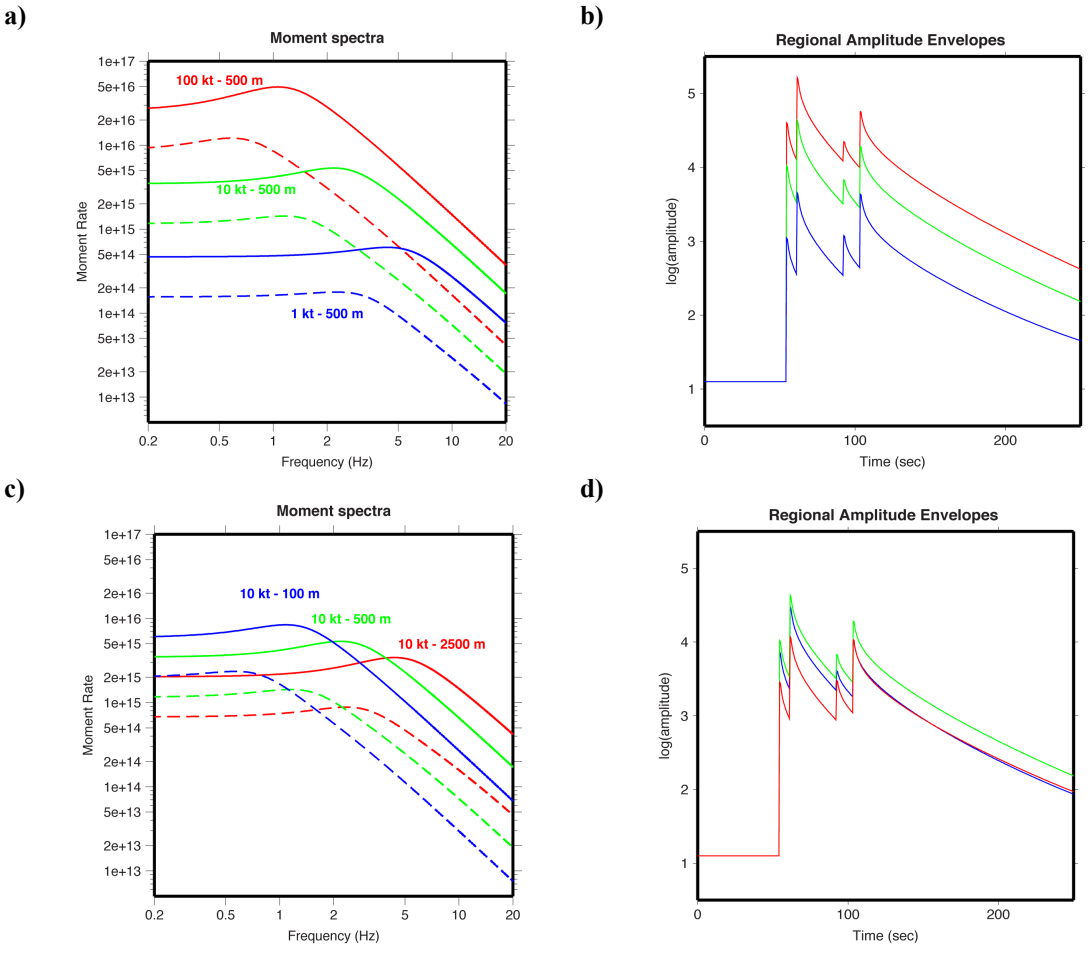

Figure 5. A comparison of moment spectra and regional amplitude envelopes from explosion sources of varying yield (a, b) and varying depth (c, d). In the moment spectra plots (a, c), the solid lines indicate P-wave spectra and dashed lines indicate S-wave spectra. Regional amplitude envelopes are shown for the 2-3 Hz passband. The color of the envelopes in panels b and d refer to the corresponding sources indicated in panels a and c. Figure from Pasyanos et al. (2012b).

This sensitivity of the envelopes to source parameters allows us to estimate these parameters by minimizing misfit. We perform a grid search of 2006 and 2009 DPRK tests for variable yield and depth of burial (DOB) assuming the same source type and material. We perform a search ranging from 0.01 to 100 ktons in yield and from 10 to 1000 m in depth at every first significant digit of 1, 2, and 5. We used both station MDJ and TJN using the 1-1.5, 2-3, 4-6, and 6-8 Hz frequency bands. Misfits were calculated using log-amplitudes, which emphasizes reducing the misfit of the coda relative to the higher-amplitude direct phases. Results are shown in Figure 6, along with a standard depth of burial estimated for Kazakhstan (Israelsson, 1994). For the 2006 event, a minimum misfit is found at a yield of 500 tons (200-800 tons) and a DOB of 100 m (20-300 m). For the 2009 event, the minimum occurs at a yield = 2 ktons (1-5 ktons) and DOB = 200 m (70-600 m). These are consistent with the analysis reported by the Director of National Intelligence (DNI). The yield estimate depends on the particular explosion model used and other authors have found different estimates (Figure 6).

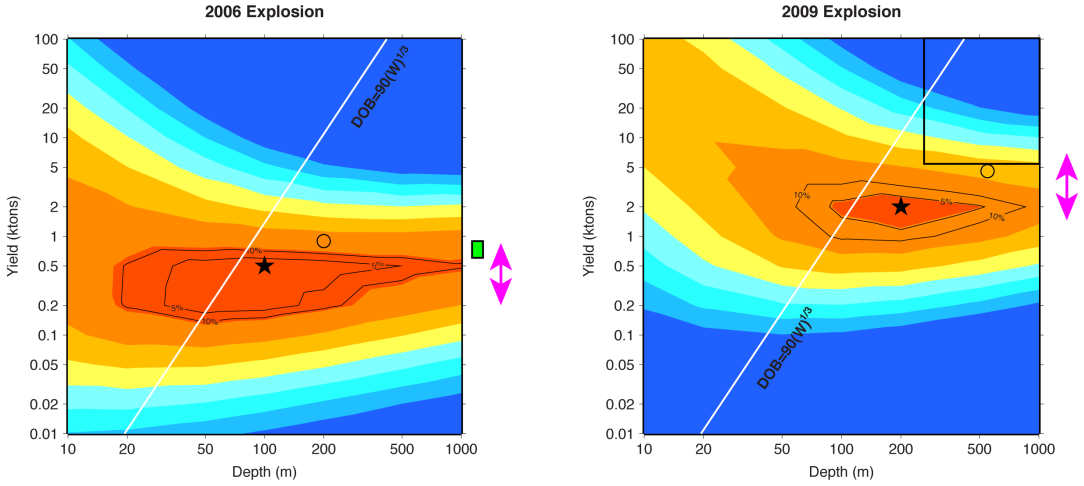

Figure 6. Misfit of the 2006 and 2009 events as a function of depth of burial and explosive yield assuming the Mueller-Murphy model, granite shot point and the Fisk conjecture. The minimum RMS is indicated with the star. Contours of 5% and 10% above the minimum are drawn. The line shows a standard depth of burial of 90 $(W)^{1/3}$ (Israelsson, 1994). Other symbols on figures represent estimates from other studies (not discussed here). Figure from Pasyanos et al. (2012b)

While we cannot independently confirm the validity of these values for the DPRK tests, the methodology has also been tested on explosions at the Nevada Test Site (NTS), where the true depth and yield were reported. Figure 7 shows the RMS misfit of the Atrisco event recorded at station ELK (Elko, Nevada). The minimum misfit (indicated by the star) occurs at a depth of 500 m and a yield of 100 ktons, which compares favorably to the depth of 640 m and yield of 138 ktons reported in Springer et al. (2002).

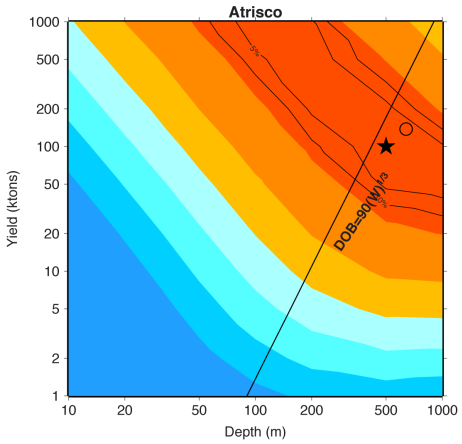

Figure 7. Misfit of the Atrisco event as a function of depth of burial and explosive yield assuming the M-M model, granite shot point and Fisk conjecture. The minimum RMS is indicated with the star. The line shows a standard depth of burial of 90 $(W)^{1/3}$ (Israelsson, 1994). The circle indicates the true yield and depth values from the report of Springer et al. (2002). Figure from Pasyanos et al. (2012b)

Capability Analysis

We can use our regional attenuation models, along with associated earthquake and explosion source models, to predict expected signal-to-noise at a station for a given combination of phase, frequency, path, magnitude, etc. Figure 8 shows an example of maps with predicted signal-to-noise of an Mw 4.0 earthquake recorded at station UOSS in Sharjah, UAE using an average noise level for the station. The panel to the left shows SNR for Sn in the 2-4 Hz passband, while the panel to the right shows 2-4 Hz Lg. Plotted on top are observed signal-to-noise from events with magnitudes around 4.0. There is some variation in the observations due to changes in the background noise level and the individual event magnitudes sometimes being slightly higher or lower than magnitude 4.0.

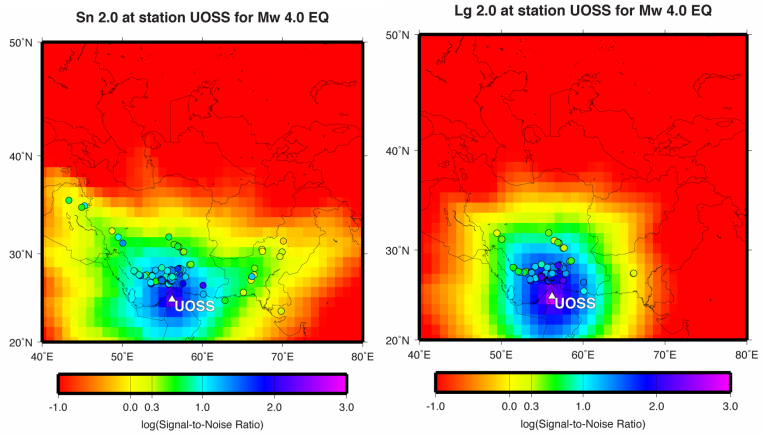

Figure 8. Expected signal-to-noise of an Mw 4.0 earthquake recorded at station UOSS in Sharjah, UAE for 2-4 Hz Sn and Lg. Colored symbols show observed SNR from events.

While magnitudes can be estimated from direct phase amplitudes, measuring them on coda provides stability to the magnitude estimate. Figure 9 show a comparison of estimated signal-to-noise for both the direct *Sn* and *Sn*-coda, in the same 2-4 Hz passband. The coda figure shows the smaller area in which a reliable magnitude estimate can be made. Here we use 60 seconds of coda, which results in an interstation standard deviation of 0.10 magnitude units (*e.g.*, Figure 13 from Mayeda et al., 2003). Longer coda windows would have lower uncertainties, while shorter windows would have higher uncertainties.

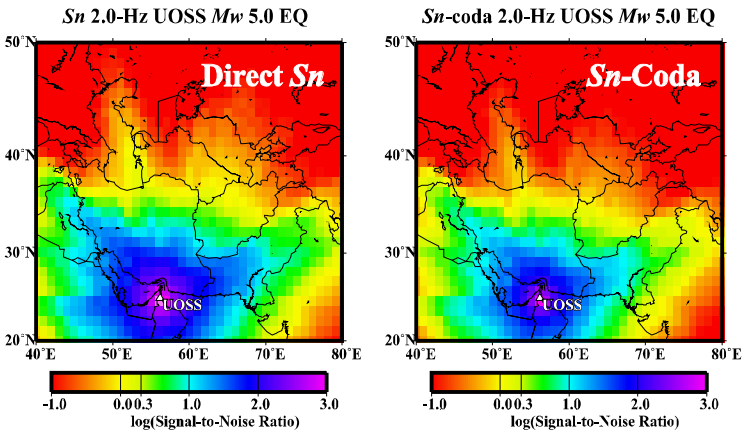

Figure 9. A comparison of estimated signal-to-noise ratios for Sn and Sn-coda in the 2-4-Hz passband from Mw 5.0 event recorded at station UOSS. The panel to the left shows the SNR of the direct phase, while the panel to the right shows the SNR of Sn-coda that has decayed 60 seconds from the direct phase.

CONCLUSIONS AND RECOMMENDATIONS

For many years, we have been building, developing, and improving all of the components that can allow us to construct the envelopes of regional phases out to observing stations from arbitrary events. These components include earthquake and explosion source models, travel time models for predicting arrivals, attenuation models that can account for the propagation, and coda decay parameters that predict the falloff that accounts for the envelope shape. Here, we integrate all of this work to allow us to estimate magnitude (or explosive yield), identify events as earthquakes or explosions, and assist in station and network capability assessments. While we will continue to improve the constitutive source, velocity, attenuation, and coda models, the integrated approach can be used now in explosion monitoring applications.

ACKNOWLEDGMENTS

We thank Stan Ruppert, Terri Hauk, Doug Dodge, and Mike Ganzberger for maintaining the LLNL Seismic Research Database and development of tools. We thank Gene Ichinose for the regional moment magnitudes used in the coda calibration. This work performed under the auspices of the U.S. Department of Energy by Lawrence Livermore National Laboratory under Contract DE-AC52-07NA27344. This is LLNL contribution LLNL-PROC-******.

REFERENCES

Baker, D., W.-Y. Kim, H. Patton, G. Randall, and P. Richards (2009). Improvements to a major digital archive of seismic waveforms from nuclear explosions: The Borovoye seismogram archive, in Proceedings of the 2009 Monitoring Research Review: Ground-Based Nuclear Explosion Monitoring Technologies, LA-UR-09-05276, 12-21.

Brune, J., (1970). Tectonic stress and the spectra from seismic shear waves earthquakes, *J. Geophys. Res.*, **75**, 4997-5009.

Denny, M.D. and L.R. Johnson (1991). The explosion seismic source function: Models and scaling laws reviewed, in *Explosion Source Phenomenology*, *AGU Monograph,* 65: ed. S. Taylor et al., 1–24.

Fisk, M.D. (2006). Source spectral modeling of regional P/S discriminants at nuclear test sites in China and the Former Soviet Union, Bull. Seism. Soc. Amer., 96, 2348-2367.

Ford, S., W. Walter, S. Ruppert, E. Matzel, T. Hauk, and R. Gok, (2010). Toward an Empirically-Based Parametric Explosion Spectral Model, in Monitoring Research Review: Ground-Based Nuclear Explosion Monitoring Technologies, LA-UR-10-05578.

Ford, S., W.R. Walter, S.D. Rupppert, E.M. Matzel, T.F. Hauk, and R. Gok (2012). An empirically-based parametric explosion spectral model, this meeting.

Israelsson, H. (1994). Analysis of historical seismograms – root mean square Lg magnitudes, yields, and depth of explosions at the Semipalatinsk Test Range, *Geophys. J. Int.,* 117, 591-609.

Kim, W.-Y. and G. Ekstrom (1996). Instrument responses of digital seismographs at Borovoye, Kazakhstan, by inversion of transient calibration pulses, *Bull. Seism. Soc. Amer.*, 191-203.

Mayeda, K., A. Hofstetter, J.L. O'Boyle, and W.R. Walter (2003). Stable and transportable regional magnitudes based on coda-derived moment-rate spectra. *Bull. Seismol. Soc. Am.*, 93, 224-239.

Mayeda, K. and W.R. Walter (1996). Moment, energy, stress drop, and source spectra of western U.S. earthquakes, *J. Geophys. Res.,* 101, 11195-11208.

Mueller R.A. and J.R. Murphy (1971). Seismic characteristics of underground nuclear detonations: Part I. seismic spectrum scaling, *Bull. Seism. Soc. Amer,* 61, 1675-1692.

Pasyanos, M.E. and W.R. Walter (2009). Improvements to regional explosion identification using attenuation models of the lithosphere, *Geophys. Res. Lett.,* doi:10.1029/2009GL038505.

Pasyanos, M.E., E.M. Matzel, W.R. Walter, and A.J. Rodgers (2009a). Broad-band Lg attenuation modeling of the Middle East, *Geophys. J. Int.,* 177, 1166-1176, doi:10.1111/j.1365-246X.2009.04128.x

Pasyanos, M.E., W.R. Walter, and E.M. Matzel (2009b). A simultaneous multi-phase approach to determine P-wave and S-wave attenuation of the crust and upper mantle, *Bull. Seism. Soc. Amer.*, 99-6., 3314-3325, doi:10.1785/0120090061.

Pasyanos, M.E., W.R. Walter, and K.M. Mayeda (2012). Exploiting regional amplitude envelopes: a case study for earthquakes and explosions in the Korean Peninsula, *Bull. Seism. Soc. Amer.*, in press.

Pasyanos, M.E., S.R. Ford, and W.R. Walter (2012). Testing event discrimination over broad regions using the historical Borovoye Observatory explosion dataset, submitted to *Pure and Applied Geophysics*.

Walter, W.R. and S.R. Taylor (2001). A revised magnitude and distance amplitude correction (MDAC2) procedure for regional seismic discriminants: theory and testing at NTS, Lawrence Livermore National Laboratory, UCRL-ID-146882, http://www.llnl.gov/tid/lof/documents/pdf/240563.pdf